frontiers in Physics

ORIGINAL RESEARCH
published: 14 July 2020
doi: 10.3389/fphy.2020.00219

Experimental Investigation, Modeling, and Optimization of Wear Parameters of B_4C and Fly-Ash Reinforced Aluminum Hybrid Composite

*Mohit Kumar Sahu and Raj Kumar Sahu**

Department of Mechanical Engineering, National Institute of Technology Raipur, Raipur, India

OPEN ACCESS

Edited by:
Jinjin Li,
Shanghai Jiao Tong University, China

Reviewed by:
Keshavamurthy R,
Dayananda Sagar College of Engineering, India
Satnam Singh,
The Northcap University, India
Gai Zhao,
Nanjing University of Aeronautics and Astronautics, China

***Correspondence:**
Raj Kumar Sahu
raj.mit.mech@gmail.com

Specialty section:
This article was submitted to Computational Physics, a section of the journal Frontiers in Physics

Received: *06 March 2020*
Accepted: *22 May 2020*
Published: *14 July 2020*

Citation:
Sahu MK and Sahu RK (2020) Experimental Investigation, Modeling, and Optimization of Wear Parameters of B_4C and Fly-Ash Reinforced Aluminum Hybrid Composite. Front. Phys. 8:219. doi: 10.3389/fphy.2020.00219

Lightweight and high-wear performance materials are currently in demand for various advanced applications in areas such as aerospace and automobiles. These demands can be achieved by hybrid aluminum matrix composites (HAMCs), as they possess excellent mechanical and tribological properties which can be customized using more than one reinforcement. Boron carbide (8 wt.%) and fly-ash (2 wt.%) reinforced hybrid aluminum 7075 composite was successfully fabricated using a stir-casting route. Wear is a crucible phenomenon that occurs over the interaction of surfaces and affects the performance of the material. To investigate wear behavior of developed HAMC, dry sliding wear tests were conducted based on the central composite design, taking the specific wear rate as a response parameter. Modeling of wear parameters is crucial, as it helps to predict the value of the wear response at the given set of input parameters without performing experimentation. Response surface method (RSM) was used for the modeling of wear parameters to develop an empirical model of specific wear rate in terms of load, sliding speed, and sliding distance. The high value of the coefficient of determination ($R^2 = 0.9894$) illustrates the goodness of fit of the developed model. Moreover, the optimal condition of wear parameters was determined as 20 N load, 1.5 m/s sliding speed, and 500 m sliding distance; the predicted value of specific wear rate in this set of parameters is 0.2×10^{-5} mm^3/N-m. The validation test at optimal conditions was performed and the specific wear rate was found to be 0.205×10^{-5} mm^3/N-m, which shows good agreement with the predicted value. The worn-out surface and debris were analyzed using scanning electron microscope (SEM) images and electron dispersive spectrums (EDS) to completely explore the mechanism of wear.

Keywords: hybrid aluminum matrix composites, stir casting, dry sliding wear, specific wear rate, response surface method

INTRODUCTION

Wear is a phenomenon of material removal that occurs in the interface between two surfaces, which affects the reliability and durability of any machine [1, 2]. Whereas, the strength to weight ratio of the material directly affects the power consumption and efficiency of any mechanism [3]. Therefore, wear and strength to weight ratio are crucial properties of materials needed to enhance the performance of any machine or mechanism. The requirement of these properties compel the developments of high strength to weight ratios and high wear-resistant composites. Aluminum composites are suitable materials to meet these properties. Particulate aluminum matrix composites (AMCs) exhibit high tensile and compressive strength and better tribological properties than conventional materials. Besides, the properties of AMCs cannot be customized due to single reinforcements available in the composite. However, hybrid aluminum matrix composites (HAMCs) have the accessibility to customize the properties as per requirements by choosing appropriate reinforcements. Due to this accessibility and the perfect blend of customizable tribological and mechanical properties, high strength-weight ratio, and environmental well-being, HAMCs have become a prime choice for aerospace, automobile, sports, and electronics industries [4–7]. These composites are capable of replacing high-cost monolithic materials or single reinforced materials in advanced applications. There are three main categories of HAMCs: two different synthetic ceramic reinforced HAMCs; synthetic ceramics and agro-waste derivatives reinforced HAMCs; synthetic ceramics and industrial waste reinforced HAMCs [8]. Hybrid composites with synthetic ceramics and industrial waste by-products have been found to be suitable for advanced applications in automobiles, aerospace, and structural applications due to their lightweight' low-cost, and high strength [9, 10]. Such composites also save on natural resources and lead to a green and clean environment by utilizing industrial waste as reinforcements [11]. In this type of composite, the selection of material plays a key role in the composite's properties.

The selection of base aluminum alloy is the foremost criteria. The yield and ultimate tensile strength of various aluminum alloys are listed in **Table 1**, where aluminum alloy 7075 shows the highest value of yield and ultimate tensile strength as compared to the other grades of aluminum alloys. Moreover, it is a light-weight and high-temperature resistant alloy, which makes it preferable for use in automotive, aeronautical, sports, and electronics applications [13, 14]. Therefore, aluminum 7075 alloy was selected as the matrix material for the hybrid composite. There are also three categories of reinforcements used in aluminum composites: synthetic ceramics, industrial waste, and agro-waste [8, 15]. In hybrid composites, primary reinforcement mainly focuses on strength enhancement. Synthetic ceramics are used as primary reinforcements as they possess a superior strength compared to other types of reinforcements. On the other hand, the secondary reinforcement reduces the cost and the weight of the hybrid composite as they are freely available and have a lower density [16, 17]. The combination of synthetic ceramics with industrial waste leads to lightweight, inexpensive, high-strength hybrid composites, which makes them suitable for advanced applications [18, 19].

TABLE 1 | Tensile strength of various grades of aluminum alloys [12].

Grades of aluminum alloys	Tensile strength	
	YS (MPa)	UTS (MPa)
AA7075	505	570
AA 6061	145	240
AA 2024	325	470
AA 1100	35	90
AA 295.0	110	221
AA 5052	195	230
AA 359.0	164	228
AA 8090	360	465
AA 3003	40	110
AA 2090	455	455

In the synthetic ceramics category, B_4C, SiC, Al_2O_3, TiC, TiB_2, SiO_2, etc. are the most commonly used reinforcements due to their significant property enhancement when reinforced with aluminum [19, 20]. Properties of majorly used ceramics were compared and shown in **Table 2**. Out of these, boron carbide possesses the lowest density and highest elastic modulus compared to other listed ceramics. It also shows better interfacial bonding and excellent wear performance when reinforced with aluminum. Moreover, hardness of B_4C is just below that of diamond (9.5+ in Mohs' scale) and possesses good thermal conductivity of 30–42 $Wm^{-1}K^{-1}$, good thermal stability, a very high melting point of 2,445°C, and high electrical conductivity of 140(s) at 25°C [9, 17, 18, 21, 22, 29, 30]. Furthermore, incorporation of boron carbide with Al7075 enhances the specific strength, specific stiffness, mechanical properties, and wear resistance of the composite [23, 31]. These exceptional properties made boron carbide a good choice as a primary reinforcement for advanced applications in automotive, armaments, aircraft, and aerospace applications, especially for those parts which are subjected to very high temperatures and require high abrasion resistance [32–35].

In the industrial waste category, fly-ash, and red mud are the most commonly used reinforcements as they are comprised of SiO_2 and Al_2O_3 content, which are responsible for the property enhancements of the composite [36, 37]. The comparison between fly-ash and red mud is shown in **Table 3**. This table illustrates that fly-ash has a lower density than the red mud, which is a key criteria for secondary reinforcement. Fly-ash is very rich in SiO_2 and Al_2O_3 contents compared to red mud. Moreover, reinforcing fly-ash with Al alloys reduces the density and enhances the mechanical and tribological properties of the composite without increasing the cost [9, 37, 38, 43, 44]. This makes fly-ash suitable for use as secondary reinforcements for the hybrid composites. Considering above all, Al7075 was chosen as the matrix material with boron carbide and fly-ash as primary reinforcement and secondary reinforcement, respectively. Three to ten micron-sized irregular shape B_4C powder and sphere shapes of fly-ash were used as reinforcements. Apart from the material selection, the processing route and its parameters also play a vital role in the properties of the developed composite.

TABLE 2 | Properties of various ceramics reinforcements.

Ceramics reinforcements	Density ($\times 10^3$ kg m^{-3})	Elastic modulus (GPa)	Interfacial bonding and chemical stability	Wear performance when reinforced with aluminum	References
B_4C	2.52	448	Excellent	Excellent	[9, 12, 17, 18, 21–24]
SiC	3.21	324	Good	Good	[12, 24]
Al_2O_3	3.98	379	Moderate	Good	[12, 24]
TiC	4.93	269	Good	Excellent	[12, 25, 26]
TiB_2	4.50	414	Good	Good	[12, 27]
SiO_2	2.66	73	Good	Good	[12, 28]

TABLE 3 | Comparison of fly-ash and red mud.

Industrial waste reinforcements	Density	SiO_2 content	Al_2O_3 content	Wear performance when reinforced with aluminum	References
Fly-ash	Low	Very high	High	High	[10, 11, 38–40]
Red Mud	High	Moderate	Moderate	Moderate	[11, 19, 41, 42]

Stir casting is an economical route of composite preparation and offers ease of production; due to these properties it was used by various authors for the processing of AMCs and HAMCs [18, 24, 43, 45–48]. Therefore, the stir casting route was used in the current research for fabrication of hybrid composites. In this method, wettability of reinforcements with the matrix alloy is a major problem [49, 50]. This problem was resolved by adding K_2TiF_6 and Mg powder in the molten aluminum, which helps to enhance the wettability of boron carbide and fly-ash with aluminum [23, 51–53]. The selection of optimal values of stirring and casting parameters is crucial as they lead to the homogeneous distribution of reinforcements, which is desired in the development of composites [45]. Stirring parameters such as impeller blade angle, impeller diameter, and stirring speed are the major influencing stirring parameters [39]. However, the position of the impeller and feed rate are other key parameters that affect the distribution of reinforcements [54]. Some literature has suggested the optimal values of these parameters, which were adopted in this research for the fabrication of hybrid composites [39, 54]. Boron carbide and fly-ash reinforced aluminum alloy monolithic and hybrid composites were fabricated by many researchers.

Baradeswaran et al. fabricated boron carbide reinforced Al 7075 composites and investigated wear behavior; they observed reduction of wear rate with the increase of boron carbide content [23]. Manikandan et al. studied the microstructure, mechanical, and tribological behaviors of B_4C and cow dung ash reinforced Al 7075 hybrid composite. They found that the hardness, tensile strength, flexural strength, and wear resistance were increased with an increase of B_4C and maximum tensile strength was achieved for 10 wt. % of B_4C [45]. Kumar et al. fabricated and evaluated wear behavior of Al/B_4C/fly-ash composites using the Taguchi method; they found a high level of bonding between matrix and reinforcements (B_4C and fly-ash) in the developed composite. Further, they concluded that the load has the most significant effect on the specific wear rate compared to other wear parameters [29]. Saravanan et al. fabricated and investigated the hardness of Al6082 alloy reinforced with boron carbide and found that the composite with 8 wt.% B_4C exhibited the highest hardness and tensile strength [55]. Arunachalam et al. fabricated AA 336/B_4C/Fly-ash composites and optimized dry sliding wear parameters for minimum weight loss. They found that weight loss increased with the increase of load and sliding distance. However, weight loss decreased with an increase in sliding velocity. The optimal values were found as 18.1 N of load, 905.4 m of sliding distance, and 4.18 m/s of sliding distance [44]. Reddy et al. investigated the mechanical and tribological aspects of Al7075/B_4C/fly-ash composite and concluded that the incorporation of B_4C and fly-ash into the Al7075 alloy tremendously enhances the micro-hardness, tensile strength, and wear resistance. Faisal et al. investigated the mechanical and wear properties of Al7075/B_4C, Al7075/B_4C/Gr, and Al7075/B_4C/Fly-ash composites and concluded that the addition of boron carbide and fly-ash in the Al7075 aluminum matrix enhances the hardness and wear resistance of the composite [56].

However, Sahu et al. [10] fabricated B_4C and fly-ash reinforced hybrid composites with varying amounts of boron carbide (2,4,6, and 8 wt. %) and a constant amount of fly-ash (2 wt.%). Microstructural characterization was done using optical micrograph, SEM images, and EDS spectrum. They confirmed the incorporation and uniform distribution reinforcements (B_4C and fly-ash) throughout the composite. Further, micro-hardness was investigated, and they found the highest micro-hardness value for Al7075/8 wt.%B_4C/2 wt.% Fly-ash hybrid composite of 123.29 HV, which was 37.2% higher than the base matrix alloy. They had proposed the investigation of tribological properties for future work. Since the hardness of the materials is one of the influencing parameters of tribological properties, high hardness leads to high wear resistance. Hence, combination of 8 wt.% boron carbide and 2 wt.% fly-ash Al7075 was selected for the tribological investigation. Moreover, modeling of wear parameters is a very useful statistical approach for the prediction

of wear response and to avoid experimentations [57, 58]. This can be accomplished by the establishment of a mathematical correlation between the wear responses and input parameters. Response Surface Method (RSM) is a perfect combination of statistical and mathematical tools for evolving, refining, and optimizing [59–61]. This technique is an extensively used and preferred tool by industries and researchers to analyze the quantitative measure of the effect of input parameters over one or more responses [60, 62]. Response Surface Method was used by various researchers and it was found to be a very useful and suitable tool for the analysis of wear parameters [57, 60].

Gajalakshmi et al. had used the response surface method coupled with gray relation analysis for the optimization of dry sliding wear parameters of AA6026. They considered load(10–40 N,), pin speed (300–600 r/min), and track diameter (60–120 mm.) as wear input parameters and suggested the optimum setting for minimal wear as 35.21 N load, 375.65 r/min speed, and 111.53 mm track diameter. Moreover, the predicted wear characteristics from the RSM model and experimental results are in close concord, and the errors lie within 3–6% [60]. Sivasankaran et al. had used the response surface method to investigate the effect of TiB2 and Gr on the sliding wear behavior of the hybrid composite. They found that the experimental results and the predicted wear characteristics from the developed model were in good agreement [63]. Chelladurai et al. had used RSM for the optimization of wear parameters of a copper-coated steel wire-reinforced AA336 composite by considering three factors and five levels of central composite design. An empirical model was developed for weight loss; the predicted and experimental weight loss at optimal conditions (18.1 N load; 2.41 m/s velocity; 2,094 m sliding distance) were in agreement with an error percentage of ± 8%. It was found that the weight loss increases with the increase of load and sliding distance, whereas it decreases with the increase of sliding speed [23]. Baradeswaran et al. used RSM for the modeling and optimization of wear rates of Al7075/B_4C/Gr and Al6061/B_4C/Gr hybrid composites. They found an optimal condition of parameters for the minimum wear rate as load (10 N), sliding speed (0.8 m/s), and sliding distance (2,000 m). They found the AA7075 hybrid composite exhibits better wear performance than base alloys and AA 6061 hybrid composite under the optimal conditions [58].

It has been observed from the above literatures that the Al7075/8 wt.%B_4C/2 wt.%fly-ash hybrid composite possesses the highest hardness (123.29 HV) among its group of composites fabricated by Sahu et al. [10]. Tribological properties are significantly dependent on the hardness of the material. Moreover, the process parameters also affect the tribological performance. Hence, the experimental investigation, establishment of empirical correlation, and optimization of wear parameters of this composite is a promising area of research that is still untouched. The objective of this work was to develop a predictive model for specific wear rate and to determine optimal combinations of parameters for minimum specific wear rate of an Al7075/8 wt.%B_4C/2 wt.%fly-ash hybrid composite. An empirical model of wear was developed in this work, which can be used for the prediction of specific wear rate of Al7075/8 wt.%B_4C/2 wt.%Flyash composite. Moreover, optimal conditions of wear parameters (load, sliding speed, and sliding distance) were determined, which may help researchers in further investigation of the effects of temperature and lubrication of this composite in high-temperature sliding wear tests with lubrication.

EXPERIMENTAL DETAILS

Composite Preparation

Stir casting is the most prominent and economical processing route for the fabrication of hybrid aluminum matrix composites due to its ease of processing and suitability for mass production. Boron carbide and fly-ash reinforced hybrid aluminum 7075 composites (Al7075/8%B_4C/2%FA) are prepared using stir casting (SC) techniques. The schematic of the stir casting setup is shown in **Figure 1**. This setup consists of three main parts: an environment-controlled bottom pouring electric furnace with an inert gas inlet, a crucible with a bottom opening, and a stirring setup with feeder and the mold. The stir-casting process takes place in this setup using four basic stages: melting, stirring, feeding, and pouring. The melting stage comprises of heating coils in the furnace, thermocouple, and the control panel. The stirring stage involves the speed-controlled motor, stirring rod, and stirrer impeller blade. The feeder is inserted inside the furnace to feed reinforcement particles at a controlled feed rate. The inside environment is controlled by argon gas blown through a gas inlet. Thereafter, the mixed slurry of reinforcements and aluminum is poured through the bottom opening into the mold. The chemical composition of aluminum 7075 and fly-ash used is listed in **Table 4**. It can be observed that the used fly-ash is rich in SiO_2 and Al_2O_3 content i.e., 61.04 and 24.96%, respectively, and which are responsible for enhancing the properties of the composite. Magnesium (Mg) powder and potassium-hexa-fluro-titanate (K_2TiF_6) flux have been added into the melt during the stirring process as wetting agents to improve the wettability of fly-ash and boron carbide with aluminum [58, 64, 65].

Table 5 shows the list of optimal stir casting parameters that are being used for the fabrication of hybrid composites to achieve a homogeneous distribution of reinforcements and to avoid the accumulation of reinforcements into the matrix phase. The homogeneous distribution of reinforcement particles leads to the uniform property throughout the composite, which is desired in most engineering and advanced applications [39].

The steps involved in the stir casting process are preheating, melting, stirring, pouring, and solidification. Initially, the aluminum 7075 was preheated at 850°C, while simultaneously the mixture of boron carbide and fly-ash were also preheated at 300°C for 2 h [58, 64, 65, 68]. The mechanical stirrer of the impeller blade angle is 30°, the impeller blade diameter is 50% of the crucible diameter, and this is introduced in the melt and stirred at 550 rpm.

The mechanical stirring process starts the formation of a vortex in the melt, then the mixture of boron carbide and fly-ash is fed into the melt at a feed rate of 0.8–1.5 g/s; simultaneously, wetting agents were also fed at the same rate into the melt to enhance the wettability. After completion of the

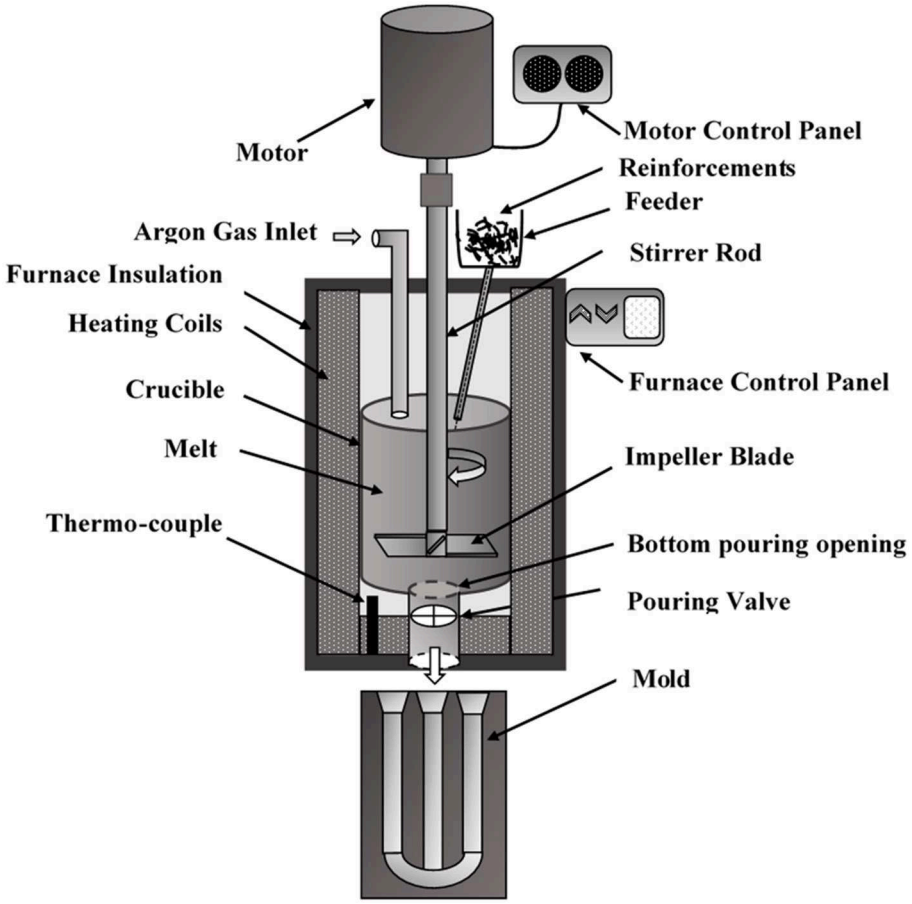

FIGURE 1 | Schematic of stir casting setup used for the fabrication of the hybrid composite.

TABLE 4 | Chemical composition of Al7075, fly-ash, and boron carbide in wt. percent.

Al 7075	Element	Zn	Mg	Cu	Fe	Si	Cr	Ni	Al
	Wt. %	5.85	2.04	1.12	0.20	0.40	0.33	O.23	Remaining
Fly-ash	Element	SiO_2	Al_2O_3	MgO	Fe_2O_3	TiO_2	CaO	K_2O	
	Wt. %	61.04	24.96	0.57	6.84	2.82	1.0	2.77	
Boron Carbide	Element	B	C						
	Wt. %	80.13	19.87						

TABLE 5 | Parameters used for the fabrication of the hybrid composite [10, 39, 54].

Selection and casting parameters	Value	References
Stirring time	10 min	[39, 54]
Angle of impeller blade	30°	[39, 54]
Diameter of impeller blade	Half of the diameter of the crucible	[39, 54]
feed rate	0.8–1.5 g/s	[39, 54]
Stirring speed	550 rpm	[39, 54, 66]
Wetting agents	K_2TiF_6 and magnesium	[23, 58, 66]
Shielding environment	Argon insert environment	[67]

feeding process, the stirring process was continued for 10 min to distribute the particles homogenously throughout the matrix phase [39, 54]. Subsequently, the slurry was poured in a preheated permanent mold made of cast iron and left for natural cooling and solidification. The fabrication, microstructural analysis, and micro-hardness of this composite are discussed in Sahu et al. [10]. After cooling, the cylindrical wear testing specimen of 9 mm diameter and 40 mm length were measured [69]. A further wear test was carried out based on the central composite design.

Dry Sliding Wear Test

The dry sliding wear test was performed using a Pin on Disc test rig (Model: *TR-20LE-PHM400-LHM600)* with the disc material EN31 steel of hardness 860 HV and initial surface roughness of 0.1 Ra (micrometers) [70]. In this investigation, the specific wear rate was selected as the wear response parameter. Whereas, load, sliding speed, and sliding distance were chosen as input

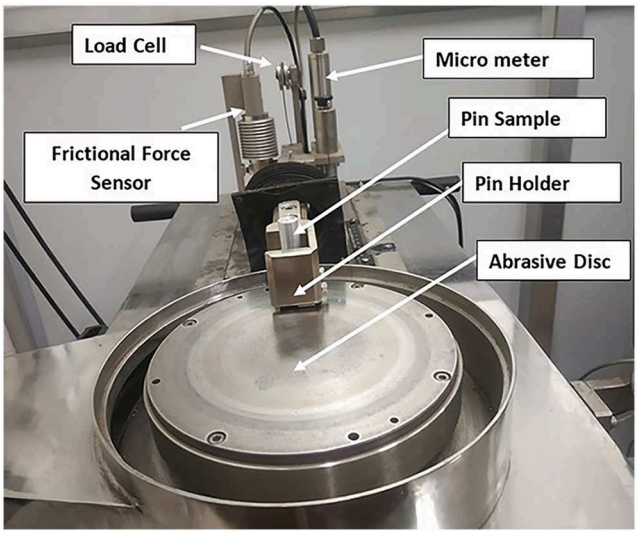

FIGURE 2 | Pin on disc dry sliding wear test rig.

parameters [58, 71, 72]. The sliding wear parameters range were selected as load: 10–50 N; sliding distance: 500–1,500 m; sliding speed: 0.5–1.5 m/s, based on previous literature [29, 39, 44, 58, 70, 73]. Further, five levels of each factor were calculated as per the central composite design based on the rotability value ($\alpha = 1.682$), which was obtained using Minitab 19 software (detailed discussion in experimental design section) [62, 73, 74].

The test rig has three major elements: the pin on disc test apparatus, the controlling device, and the computer with Windocom 2010 software connected to the controlling device. The setup of the Pin on Disc testing rig is shown in **Figure 2**. This setup consists of the abrasive disc, the specimen pin holder, micrometer, frictional force sensor, and load cell. It also has a controlling device that can control the speed of the abrasive disc, time, and number of revolutions of the disc. In the controlling device, some displays show the value of wear depth and frictional force. The controller sends signals to the connected computer, which shows instantaneous readings and graphs.

Disc rotation per minute and time of rotation for each run was calculated using Equation (1) and Equation (2) for the given track diameter, sliding distance, and sliding speed, where N is rotation per minute (rpm), D is track diameter (m), t is the time of rotation (minute), and v is the velocity of the disc (m/s).

$$N = \frac{v \times 60}{\pi D} \tag{1}$$

$$t = \frac{d}{v \times 60} \tag{2}$$

The dry sliding wear tests of the pin were carried out at loads of 10, 18, 30, 42, and 50 N, at sliding speeds of 0.5, 0.7, 1.0, 1.3, and 1.5 m/s, and sliding distances of 500, 703, 1,000, 1,297, and 1,500 m, as per the experimental design matrix shown in **Table 6** [73]. All tests were performed at room temperature of 30–35°C and a relative humidity of 25–35% in the unlubricated condition of the specimen/disc interface [70]. Initially, the mass of the sample had been measured by the weighing machine with the least count of 0.0001 g. The track diameters were adjusted to 130 mm. A wear test specimen of 9 mm diameter and 40 mm length was fitted in the pin holder and the load was placed in the load cell unit, which results in continuous contact between the specimen and the counterpart. Further, the micrometer was adjusted such that the reading should be in the range of −20 to +20 to avoid error in reading, and the micrometer and frictional force reading were set to zero. The rpm and time were set using a control device and the required data were filled in on the Windocom 2010 software installed on the computer. The start button was pressed in the software and in the controlling device simultaneously. This way, the tribometers starts and the disc rotates which produces the sliding wear of the specimen. Once the test was completed, the mass of the specimen was measured to calculate the mass loss and further specific wear rate was calculated using the density of composite, load, and sliding distance. This procedure was repeated for all 20 tests.

TABLE 6 | List of Input parameters with coded and un-coded values.

Factors	Symbols coded	Encoded values of coded levels				
		−1.682	−1	0	1	1.682
Load (N)	X1	10	18	30	42	50
Speed (m/s)	X2	0.5	0.7	1.0	1.3	1.5
Sliding Distance (m)	X3	500	703	1,000	1,297	1,500

MATHEMATICAL MODELING BY RESPONSE SURFACE METHOD

Response Surface Method

The response surface method (RSM) is an advanced and powerful statistical tool. It has a perfect combination of statistical and mathematical implements for developing, refining, and optimizing which makes it suitable for this research to model wear behavior of the developed composite [57, 75]. The specific wear rate was taken as the response parameter in this investigation. Response Surface Method (RSM) was used to develop an empirical model of specific wear rate (SWR). The steps involved in the response surface method are shown in **Figure 3**, which shows the identification of essential parameters and their range, formation of the design matrix, experimentation, development of the empirical model, examination of the data set, and acceptability of the developed model.

The initial two steps of the response surface method are recognizing the influencing input parameters and identifying their ranges. The influencing parameters are recognized as load, sliding speed, and sliding distance. The range of load, sliding speed, and sliding distance were identified as 10–50 N, 0.5–1.5 m/s, and 500–1,500 m, respectively.

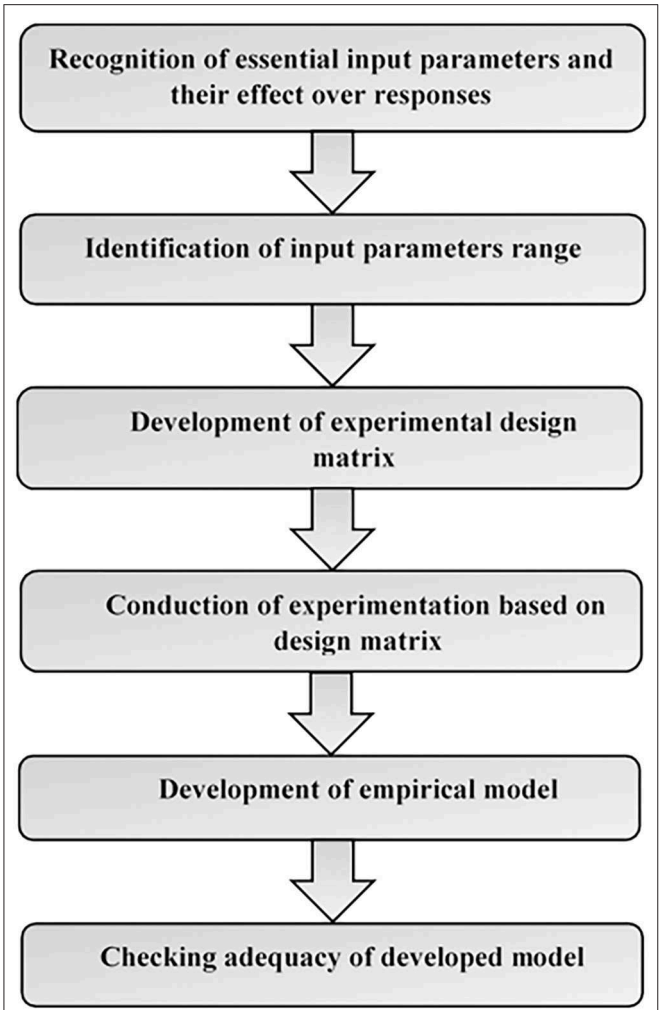

FIGURE 3 | Steps and scheme of Response Surface Method.

Experimental Design

Central composite design (CCD) is a factorial or fractional factorial design that is able to fit the full quadratic model because of the design consists of a center and axial (star) points. The development of the experimental design matrix was done using the central composite design with a 20 run test and design rotability (α) of 1.682 under the RSM technique in Minitab 19 [73, 74]. The design matrix is constructed based on five levels of three input parameters i.e., load, sliding speed, and sliding distance, using the central composite design. Further pin on disc dry sliding tests were carried out based on the design matrix.

The procedure of pin on disc wear test is described in section Dry Sliding Wear Test. These steps were repeated for all 20 experiments as per the experimental design matrix. Further, the specific wear rate was calculated using Equation (3).

$$SWR = \frac{V_L}{F \times D} \tag{3}$$

Where SWR is the specific wear rate (mm^3/Nm), F is the applied load in the load cell, and D is the sliding distance. The uncoded design matrix, as per the central composite design and calculated specific wear rate (SWR), is listed in **Table 7**. The table shows the respective specific wear rate calculated from the pin on disc dry sliding wear test for three key process parameters: load, sliding distance, and sliding speed.

RESULTS AND DISCUSSION

Mathematical Model

Modeling of wear parameters is the process of developing a correlation between wear response and the influencing parameters. This helps to avoid experimentation in the given set of parameters and predict response. Second-order polynomial multiple regression equation was developed and used to explain the mathematical relationship between the input parameters and specific wear rate [76]. This equation of specific wear rate in terms of load, sliding speed, sliding distance, and their interaction were taken for the regression analysis. All input parameters and their interactions, except for quadratic interaction sliding distance, were found as significant parameters for the specific wear rate. The significance of all coefficients was tested at the 95% confidence level using fisher's *F*-test using Minitab 19. After the determination of significant parameters, the wear models were developed using only significant coefficients which can be used to estimate the specific wear rate.

The mathematical expression for the specific wear rate with the variables is shown below in Equation (4),

$$\begin{aligned} &Specific\ Wear\ Rate\ (\times 10^{-5} mm^3/N - m) = -0.200 \\ &+0.0944\ (X_1) - 2.508\ \ (X_2) + 0.002056\ (X_3) \\ &+0.001733\ (X_1 * X_1) - 0.867\ \ (X_2 * X_2) + \ 0.0341\ (X_1 * X_2) \\ &+0.000060\ (X_1 * X_3) + 0.001279\ \ (X_2 * X_3) \end{aligned} \tag{4}$$

where X_1 = Load (N), X_2 = Sliding Speed (m/s), and X_3 = Sliding Distance (m).

Examination of Data Set and Acceptability of the Developed Model

Data Set Normality

The normal distribution of the data set can be examined by the graphical representation of the normal probability plot, which is shown in **Figure 4A** for the specific wear rate. It was observed that residual data sets were lying approximately on the theoretical normal distribution line, which confirms the normal distribution of residuals. Moreover, the histogram of Residual vs. fit plot and residual vs. frequency plot is shown in **Figures 4B,C**, respectively.

Data Set Independency

The plot between residual and observation order is shown in **Figure 4D**, which is used to test the independence of the data [62, 77]. The residual plot with run order conceals an unproductive pattern that was observed as all the observation falls between 0.2 and −0.2.

TABLE 7 | Calculated specific wear rates for the experimental design matrix.

Trial	Coded parameters			Uncoded parameters			Specific wear rate ($\times 10^{-5}$ mm^3/N-m)
	X_1	X_2	X_3	Load (N)	Sliding speed (m/s)	Sliding distance (m)	
1	−1	−1	−1	18	0.7	703	2.9094
2	1	−1	−1	42	0.7	703	9.3150
3	−1	1	−1	18	1.3	703	1.3310
4	1	1	−1	42	1.3	703	8.0626
5	−1	−1	1	18	0.7	1,297	4.9568
6	1	−1	1	42	0.7	1,297	12.0552
7	−1	1	1	18	1.3	1,297	3.6692
8	1	1	1	42	1.3	1,297	11.4236
9	−1.682	0	0	10	1.0	1,000	1.3961
10	1.682	0	0	50	1.0	1,000	13.1611
11	0	−1.682	0	30	0.5	1,000	7.3111
12	0	1.682	0	30	1.5	1,000	5.4261
13	0	0	−1.682	30	1.0	500	4.3611
14	0	0	1.682	30	1.0	1,500	8.6111
15	0	0	0	30	1.0	1,000	6.5201
16	0	0	0	30	1.0	1,000	6.7411
17	0	0	0	30	1.0	1,000	6.4811
18	0	0	0	30	1.0	1,000	6.4711
19	0	0	0	30	1.0	1,000	6.5131
20	0	0	0	30	1.0	1,000	6.7611

Analysis of Variance (ANOVA)

Analysis of variance technique (ANOVA) was used to test the significance of the developed model. Suitability of the model is determined by the coefficient of determination (R^2) [62, 77]. The coefficient of determination (R^2) for current analysis 0.9894, which shows <2% of the deviations, remained unexplained by this model. The Adjusted R^2 value is 0.9889, which is again great value and shows the high significance of the developed model. There is also a good agreement between the predicted and adjusted determination coefficients. The model is determined as significant as the value of probability was found to be less than the *F*-value [62, 78, 79]. Analysis of variance (ANOVA) is shown in **Table 8**. The value of P is <0.05 which shows that the model has a predictability of 95% confidence level. The value of the determination coefficient is 0.9894, which shows the developed model shown in Equation 4 is highly reliable. The computed value of *F* is 1882.73 which is more than the tabular value, which shows significant treatment. Hence, the proposed model is appropriate and efficient for this investigation. Moreover, the model is statistically significant as the $P < 0.05$ [80].

Effect of Wear Parameters on the Specific Wear Rate

The effect of input parameters on specific wear rate (SWR) in terms of three-dimensional surface and two-dimensional contour plots are shown in **Figures 5A–F**. The contour and surface plot of specific wear rate w.r.t. load and sliding distance is shown in **Figures 5A,B**, respectively. It has been observed from these plots that the specific wear rate increases with load and sliding distance. The highest value of specific wear is observed in the region where the load is 50 N and the sliding distance is 1,500.

Contour and surface plots between sliding speed and sliding distance are shown in **Figures 5C,D**, respectively. The figure shows that the specific wear rate increases with sliding distance and vice versa in case of sliding speed. The maximum value specific wear is observed in the region where sliding distance is 1,500 m and sliding speed is 0.5 m/s. whereas, minimum value can be seen in the region where sliding distance is 500 m and the sliding speed is 1.5 m/s.

Further, the contour and surface plot concerning sliding speed and sliding distance are shown in **Figures 5E,F**, respectively. It can be observed from the figures that the value of the specific wear rate increases with the increase of load, while it decreases with the increase of sliding distance. The maximum value of the specific wear rate can be observed in the region where the load is 50 N for all conditions of sliding speed. Whereas, the minimum value is observed in the region where sliding speed is 0.75–1.5 m/s and load is at 10–15 N. It can be concluded that the specific wear rate increases with the increase of sliding distance and load, however, it decreases with the increase of sliding distance.

Optimization

Optimization of wear parameters was performed based on the "Smaller Is Better" theory to achieve minimum specific wear rate. Response optimizer tool under RSM method was used to accomplish optimal settings of wear parameters, which are identified as 20 N load, 1.5 m/s sliding speed, and 500 m sliding distance. Further, pin on disc wear test has again been

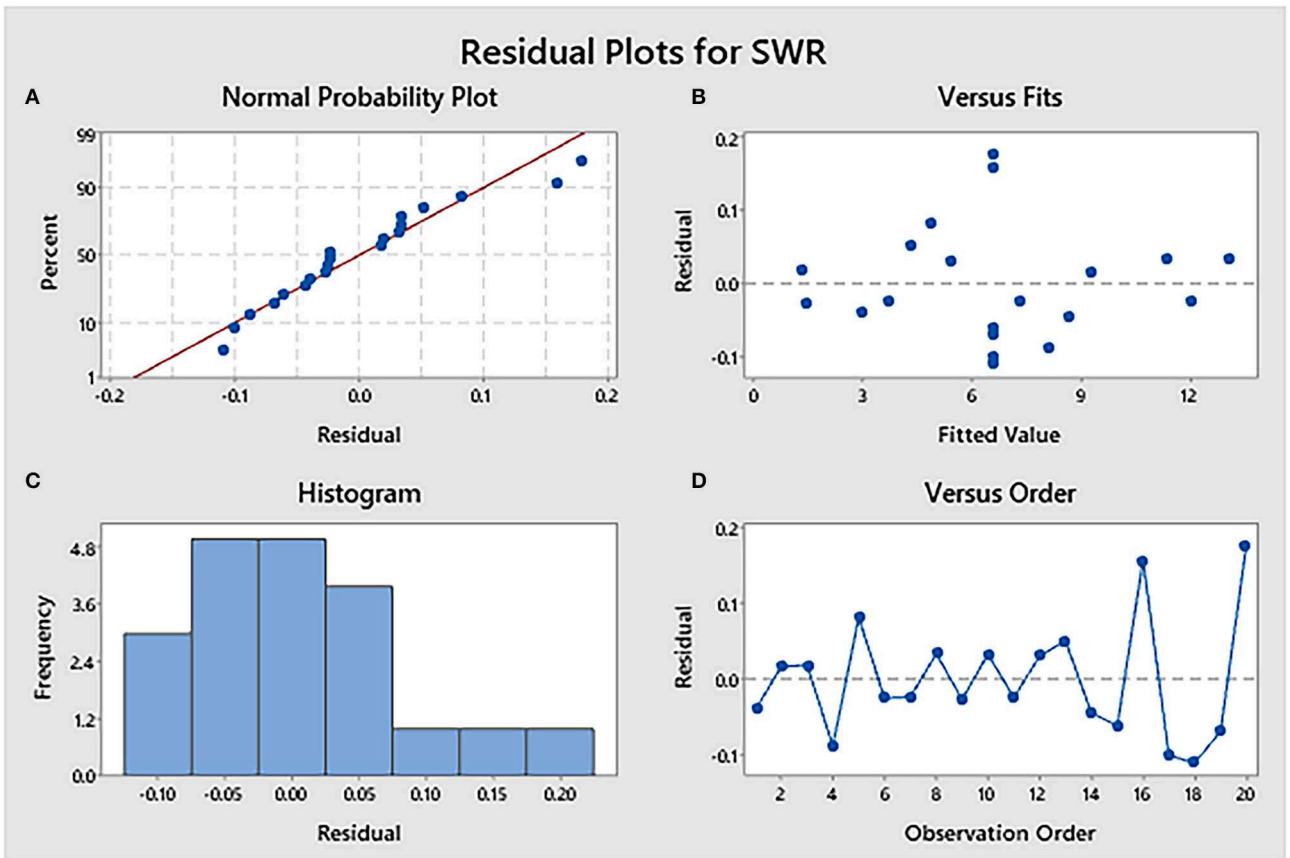

FIGURE 4 | Plots of specific wear rate: **(A)** normal probability plot, **(B)** fits vs. residual plot, **(C)** residual vs. frequency plot, and **(D)** run order plot vs. residual plot.

TABLE 8 | ANOVA table for specific wear rate.

Source	DF	Adj SS	Adj MS	*F*-value	*P*-value
Model	9	196.145	21.794	1882.73	0.000
Linear	3	194.499	64.833	5600.80	0.000
Load(N)	1	167.135	167.135	14438.44	0.000
Sliding speed(m/s)	1	4.594	4.594	396.89	0.000
Sliding distance(m)	1	22.770	22.770	1967.06	0.000
Square	3	1.053	0.351	30.33	0.000
Load(N)*Load(N)	1	0.873	0.873	75.41	0.000
Sliding speed(m/s)*Sliding speed(m/s)	1	0.085	0.085	7.38	0.022
Sliding distance(m)*Sliding distance(m)	1	0.018	0.018	1.53	0.244
2-Way interaction	3	0.592	0.197	17.06	0.000
Load(N)*Sliding Speed(m/s)	1	0.121	0.121	10.41	0.009
Load(N)*Sliding distance(m)	1	0.368	0.368	31.78	0.000
Sliding speed(m/s)*Sliding distance(m)	1	0.104	0.104	8.97	0.013
Error	10	0.116	0.012		
Lack-of-fit	5	0.027	0.005	0.31	0.888
Pure error	5	0.088	0.018		
Total	19	196.260			

Standard deviation: 0.107, R^2: 0.9894, adjusted R^2: 0.9889, Predicted R^2: 0.9882.

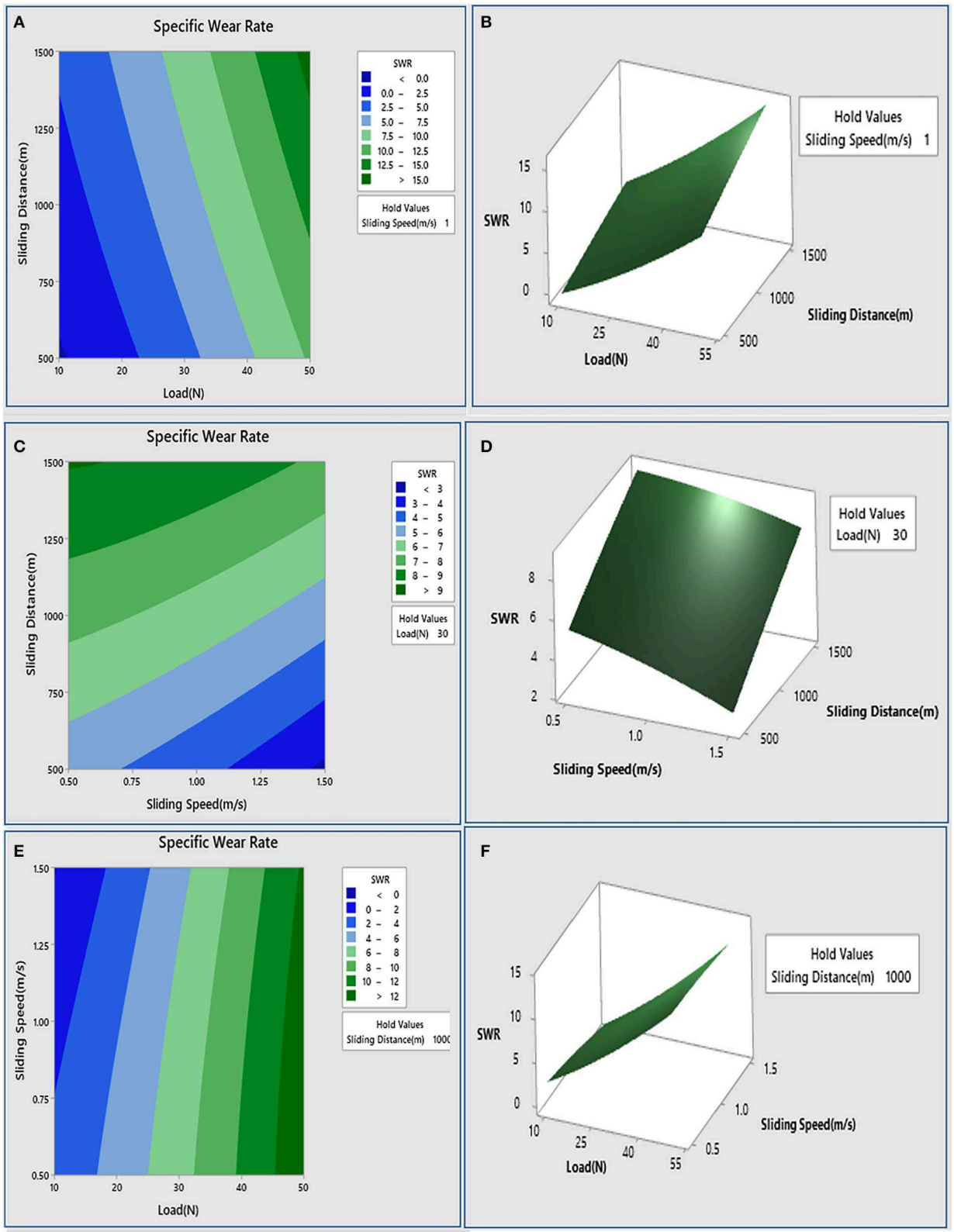

FIGURE 5 | Contour and surface plots of various parameters for specific wear rate: **(A)** contour plot for load vs. sliding speed, **(B)** surface plot for load vs. sliding speed, **(C)** contour plot for load vs. sliding distance, **(D)** surface plot for load vs. sliding distance, **(E)** contour plot for sliding distance vs. sliding speed, and **(F)** surface plot for sliding distance vs. sliding speed.

TABLE 9 | Results of confirmation test conducted at the optimal level of setting.

Response	Load(N)	Sliding speed(m/s)	Sliding distance(m)	Predicted ($\times 10^{-5}$ mm^3/N-m)	Experimental ($\times 10^{-5}$ mm^3/N-m)	Error %
Specific wear rate ($\times 10^{-5}$ mm^3/N-m)	20	1.5	500	0.200	0.205	2.5

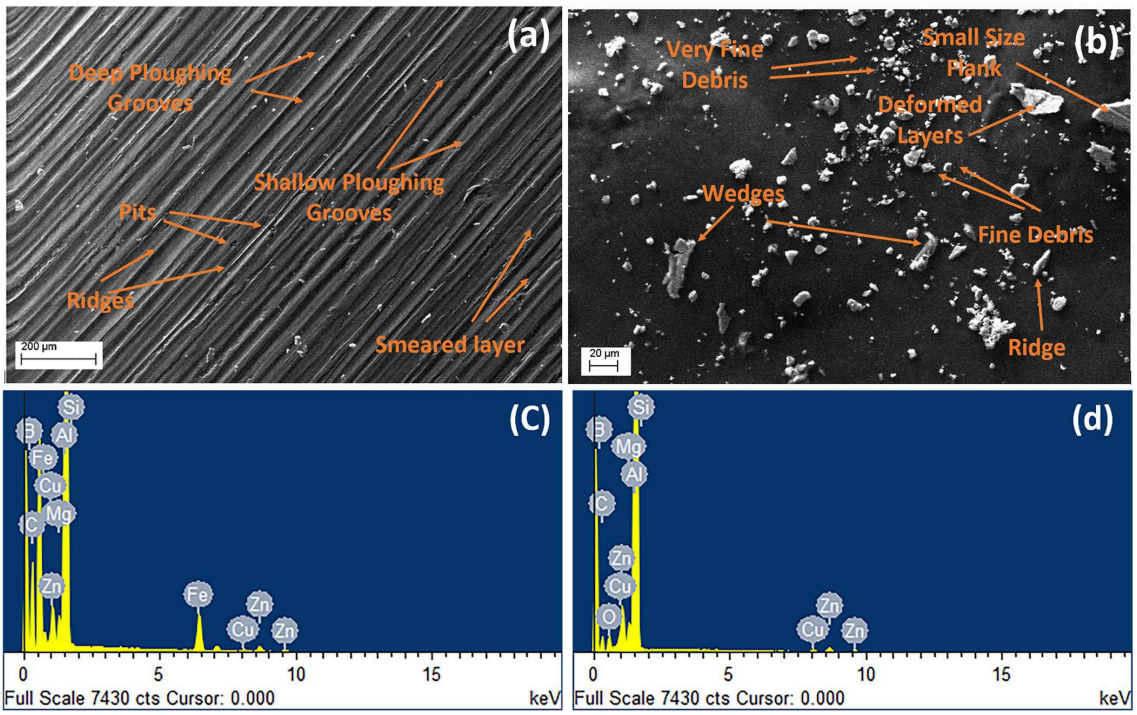

FIGURE 6 | (a) SEM images of the worn-out surface at optimal levels, **(b)** SEM images of wear debris collected during wear test at optimal levels, **(c)** EDS report of the worn-out surface at optimal levels, and **(d)** EDS of debris collected.

performed at the identified optimal level of parameters to compare experimental SWR with predicted SWR.

Validation

The experimental validation test has been conducted at the optimal set of parameters, and specific wear rate was further calculated. The specific wear rate for this test was achieved as 0.205×10^{-5} mm^3/N-m, which shows a better performance than elsewhere [81, 82]. The comparison of the predicted and experimental SWR is shown in **Table 9**. It has been found that the experimental value of SWR is slightly higher (2.25%) compared with the predicted SWR, which indicates great adaptability of this tool for wear parameters' optimization of boron carbide and fly-ash reinforced Al7075 hybrid composite.

Analysis of Worn Out Surface and Debris

Experimentation was performed at the optimal condition of setting and the analysis of worn-out surface and debris was carried out using SEM images and EDS spectrum. An SEM image of the worn-out surface is shown in **Figure 6a**, this reveals the shallow and deep plowing grooves, ridges, some pits, and a few smeared layers on the worn-out surface. Plowing grooves were formed during sliding by the asperities of the counterpart, which leads to the establishment of ridges. The repetitive sliding action caused the formation of smeared layers and the removal of some debris from ridges. Some pits were observed, which may be due to removal of reinforcement particles. During plowing, removal, and collection of some material from grooves to the tip of the asperity caused a wedge formation. This type of material removal is known as abrasive wear and the wear mechanism involved may be plowing. **Figure 6c** shows the EDS spectrum of the worn-out surface, which reveals the presence of B_4C, SiO_2, Fe_2O_3, and Al, which are the elements of matrix and reinforcement phases and shows the presence of reinforcements in the worn-out surface. The SEM image of collected debris is shown in **Figure 6b**, which reveals major amounts of debris, in the form of fine debris with some very fine debris. Moreover, few small size deformed debris and small size flacks were found, which indicates a lower specific wear rate. The EDS spectrum of debris is shown in **Figure 6d** and shows B_4C, SiO_2, and Al phase, which illustrates the matrix and reinforcement elements are present in the

debris and counter surface elements were not observed [10]. These wear phenomenon might be observed due to abrasive wear [58, 62, 69].

CONCLUSION

In the present work, B_4C (8 wt. %) and fly-ash (2 wt. %) reinforced hybrid aluminum 7075 composite was fabricated using a stir-casting route. Experimentations were conducted at different loads, sliding speeds, and distances based on a central composite design. Further, a novel wear model was developed using RSM which governs the wear performance. Based on the experimental investigation and RSM modeling, the following conclusions can be drawn:

- Modeling of wear parameters is effectively accomplished using the Response Surface Method (RSM) and Central Composite Design (CCD), and an empirical model of specific wear rate was developed which can be used for the prediction of specific wear rate at a given set of input parameters without performing experiments.
- Analysis of variance method (ANOVA) was efficiently adapted to examine the acceptability of the developed model, which gives the value of the coefficient of determination of the model.
- The coefficient of determination (R^2) is 0.9894, which means the developed model has a broad range of acceptability for B_4C and fly-ash reinforced aluminum hybrid composites.
- The optimal condition of wear parameters was determined as 20 N load, 1.5 m/s sliding speed, and 500 m sliding distance, the predicted value of the specific wear rate is 0.2×10^{-5} mm^3/N-m.
- In the validation test, the experimental value of the specific wear rate is 0.205×10^{-5} mm^3/N-m, which have only 2.25% more than the predicted rate. This result shows an excellent level of adaptability and applicability of the developed.
- Shallow and deep plowing grooves and fine debris were majorly present in the worn-out surface and debris sample, which shows evidence of abrasive wear and plowing wear mechanisms. Moreover, matrix and reinforcements elements were found on the worn-out surface and debris sample.

DATA AVAILABILITY STATEMENT

The datasets generated for this study are available on request to the corresponding author.

AUTHOR CONTRIBUTIONS

MS prepared the composite and samples. MS and RS conceived and planned the experiments. MS carried out the experiments. RS contributed to the interpretation of the results. With the guidance of RS and MS took the lead in writing the manuscript. RS provided critical feedback and helped shape the research, analysis, and manuscript. Both authors contributed to the article and approved the submitted version.

REFERENCES

1. Kato K, Adachi K. *Wear Mechanisms 7.1 7.2*. Boca Raton, FL: CRC Press (2001).
2. Sahu MK, Valarmathi A, Baskaran S, Anandakrishnan V, Pandey RK. Multi-objective optimization of upsetting parameters of Al-TiC metal matrix composites: a grey Taguchi approach. *Proc Inst Mech Eng Part B J Eng Manuf.* (2014) **228**:1501–7. doi: 10.1177/0954405413519434
3. Robert MH, Nascimento EM, Bayraktar E. *Influence of Heat Treatments on Microstructure and Mechanical Behaviour of Compressible al Matrix, Low Density Composites*. Cham: Springer (2016). doi: 10.1007/978-3-319-21762-8_17
4. Shin JH, Bae DH. Effect of the TiO2 nanoparticle size on the decomposition behaviors in aluminum matrix composites. *Mater Chem Phys.* (2014) **143**:1423–30. doi: 10.1016/j.matchemphys.2013.11.057
5. David R, Dasgupta R, Prasad BK. Effect of fine TiC particle reinforcement on the dry sliding wear behavior of *in situ* synthesized ZA27 alloy. *J Tribol.* (2019) **141**:021605. doi: 10.1115/1.4041257
6. Sugiawati VA, Vacandio F, Galeyeva A, Kurbatov AP, Djenizian T. Enhanced electrochemical performance of electropolymerized self-organized TiO2 nanotubes fabricated by anodization of Ti Grid. *Front Phys.* (2019) **7**:179. doi: 10.3389/fphy.2019.00179
7. Schöttner L, Nefedov A, Yang C, Heissler S, Wang Y, Wöll C. Structural evolution of α-Fe2O3(0001) surfaces under reduction conditions monitored by infrared spectroscopy. *Front Chem.* (2019) **7**:451. doi: 10.3389/fchem.2019.00451
8. Bodunrin MO, Alaneme KK, Chown LH. Aluminum matrix hybrid composites: a review of reinforcement philosophies; Mechanical, corrosion and tribological characteristics. *J Mater Res Technol.* (2015) **4**:434–45. doi: 10.1016/j.jmrt.2015.05.003
9. Reddy TP. Development and wear behavior investigation on aluminum-7075/B 4 C/fly ash metal matrix composites. *Adv Compos Hybrid Mater.* (2020) **3**:255–65. doi: 10.1007/s42114-020-00145-5
10. Sahu MK, Sahu RK. Synthesis, microstructure and hardness of Al 7075/B4C/Fly-ash composite using stir casting method. *Mater Today Proc.* (2019) **27**:2401–6. doi: 10.1016/j.matpr.2019.09.150
11. Wang X, Zhang N, Zhang Y, Liu J, Xiao X, Meng K, et al. Multiple flocculant prepared with dealkalized red mud and fly ash: properties and characterization. *J Water Process Eng.* (2020) **34**:101173. doi: 10.1016/j.jwpe.2020.101173
12. Wilam D. Callister DGR. *Materials Science and Engineering: An Introduction*. Vol. 7. New Delhi: Wiley India Private Ltd (2007). p. 665–715.
13. Ezatpour HR, Parizi MT, Sajjadi SA, Ebrahimi GR, Chaichi A. Microstructure, mechanical analysis and optimal selection of 7075 aluminum alloy based composite reinforced with alumina nanoparticles. *Mater Chem Phys.* (2016) **178**:119–27. doi: 10.1016/j.matchemphys.2016.04.078
14. Imran M, Khan ARA. Characterization of Al-7075 metal matrix composites: a review. *J Mater Res Technol.* (2019) **8**:3347–56. doi: 10.1016/j.jmrt.2017.10.012
15. Singh J, Chauhan A. Characterization of hybrid aluminum matrix composites for advanced applications – a review. *J Mater Res Technol.* (2015) **5**:159–69. doi: 10.1016/j.jmrt.2015.05.004
16. Michael Rajan HB, Ramabalan S, Dinaharan I, Vijay SJ. Synthesis and characterization of *in situ* formed titanium diboride particulate reinforced AA7075 aluminum alloy cast composites. *Mater Des.* (2013) **44**:438–45. doi: 10.1016/j.matdes.2012.08.008
17. Emmy Prema C, Suresh S, Ramanan G, Sivaraj M. Characterization, corrosion and failure strength analysis of Al7075 influenced with B4C and Nano-Al2O3 composite using online acoustic emission. *Mater Res Express.* (2020) **7**:016524. doi: 10.1088/2053-1591/ab6257

18. Gudipudi S, Nagamuthu S, Subbian KS, Chilakalapalli SPR. Enhanced mechanical properties of AA6061-B4C composites developed by a novel ultra-sonic assisted stir casting. *Eng Sci Technol Int J.* (2020). doi: 10.1016/j.jestch.2020.01.010. [Epub ahead of print].
19. Oluwatosin M, Keneth K, Heath L. Aluminum matrix hybrid composites: a review of reinforcement philosophies; mechanical, corrosion and tribological characteristics. *Integr Med Res.* (2015) 4:434–45. doi: 10.1016/j.jmrt.2015.05.003
20. Singh J, Chauhan A. Characterization of hybrid aluminum matrix composites for advanced applications - a review. *J Mater Res Technol.* (2016) **5**:159–69. doi: 10.1016/j.jmrt.2015.05.004
21. Sivaprasad K, Babu SPK, Natarajan S, Narayanasamy R, Kumar BA, Dinesh G. Study on abrasive and erosive wear behaviour of Al 6063/TiB2 *in situ* composites. *Mater Sci Eng A.* (2008) **498**:495–500. doi: 10.1016/j.msea.2008.09.003
22. Viala JC, Bouix J, Gonzalez G, Esnouf C. Chemical reactivity of aluminum with boron carbide. *J Mater Sci.* (1997) **32**:4559–73. doi: 10.1023/A:1018625402103
23. Baradeswaran A, Elaya Perumal A. Influence of B4C on the tribological and mechanical properties of Al 7075-B4C composites. *Compos Part B Eng.* (2013) **54**:146–52. doi: 10.1016/j.compositesb.2013.05.012
24. Shorowordi KM, Laoui T, Haseeb ASMA, Celis JP, Froyen L. Microstructure and interface characteristics of B4C, SiC and Al2O3 reinforced Al matrix composites: a comparative study. *J Mater Process Technol.* (2003) **142**:738–43. doi: 10.1016/S0924-0136(03)00815-X
25. Samer N, Andrieux J, Gardiola B, Karnatak N, Martin O, Kurita H, et al. Microstructure and mechanical properties of an Al-TiC metal matrix composite obtained by reactive synthesis. *Compos Part A Appl Sci Manuf.* (2015) **72**:50–7. doi: 10.1016/j.compositesa.2015.02.001
26. David Raja Selvam J, Dinaharan I, Rai RS, Mashinini PM. Dry sliding wear behaviour of *in-situ* fabricated TiC particulate reinforced AA6061 aluminum alloy. *Tribol - Mater Surfaces Interfaces.* (2019) **13**:1–11. doi: 10.1080/17515831.2018.1550971
27. Chen F, Chen Z, Mao F, Wang T, Cao Z. TiB2 reinforced aluminum based *in situ* composites fabricated by stir casting. *Mater Sci Eng A.* (2015) **625**:357–68. doi: 10.1016/j.msea.2014.12.033
28. Azadi M, Zolfaghari M, Rezanezhad S, Azadi M. Effects of SiO2nano-particles on tribological and mechanical properties of aluminum matrix composites by different dispersion methods. *Appl Phys A Mater Sci Process.* (2018) **124**:377. doi: 10.1007/s00339-018-1797-9
29. Kumar RA, Sait AN, Subramanian K. Evaluation of wear behaviour for Al/B4C/Fly ash composites by stir casting process. *J Sci Ind Res.* (2018) **77**:288–92. Available online at: http://nopr.niscair.res.in/handle/123456789/44289
30. Shirvanimoghaddam K, Khayyam H, Abdizadeh H, Karbalaei Akbari M, Pakseresht AH, Ghasali E, et al. Boron carbide reinforced aluminum matrix composite: physical, mechanical characterization and mathematical modelling. *Mater Sci Eng A.* (2016) **658**:135–49. doi: 10.1016/j.msea.2016.01.114
31. Gao M, Kang H, Chen Z, Guo E, Fu Y, Xu Y, et al. Enhanced strength-ductility synergy in a boron carbide reinforced aluminum matrix composite at 77 K. *J Alloys Compd.* (2020) **818**:153310. doi: 10.1016/j.jallcom.2019.153310
32. Reddy BR, Srinivas C. Fabrication and characterization of silicon carbide and fly ash reinforced aluminum metal matrix hybrid composites. In: *Materials Today: Proceedings.* Amsterdam: Elsevier Ltd (2018). P. 8374–81. doi: 10.1016/j.matpr.2017.11.531
33. Palanichamy R, Lakshmipathy J, Kulendran B, Madeshwaran V. Mechanical Characteristics of fly ash reinforced aluminum metal matrix composite-art of review. *Int J Adv Res Eng Technol.* (2019) **10**:122–9. doi: 10.34218/IJARET.10.6.2019.015
34. Zhang Y, Zhou Z, Wang J, Li X. Diamond tool wear in precision turning of titanium alloy. *Mater Manuf Process.* (2013) **28**:1061–4. doi: 10.1080/10426914.2013.773018
35. Suresh S, Moorthi NSV. Aluminium- titanium diboride (Al-TiB2) metal matrix composites: challenges and opportunities. *Procedia Eng.* (2012) **38**:89–97. doi: 10.1016/j.proeng.2012.06.013
36. Peter PI, Oki M, Adekunle AA. A review of ceramic/bio-based hybrid reinforced aluminum matrix composites. *Cogent Eng.* (2020) **7**:1727167. doi: 10.1080/23311916.2020.1727167
37. Mahanta S, Chandrasekaran M, Samanta S, Arunachalam R. Multi-response ANN modelling and analysis on sliding wear behavior of Al7075/B4C/fly ash hybrid nanocomposites. *Mater Res Express.* (2019) **6**:8. doi: 10.1088/2053-1591/ab28d8
38. Prasad SV, Asthana R. Aluminum metal-matrix composites for automotive applications: tribological considerations. *Tribol Lett.* (2004) **17**:445–53. doi: 10.1023/B:TRIL.0000044492.91991.f3
39. Sahu MK, Sahu RK. Optimization of stirring parameters using CFD simulations for HAMCs synthesis by stir casting process. *Trans Indian Inst Met.* (2017) **70**:2563–70. doi: 10.1007/s12666-017-1119-5
40. Rohatgi PK, Kim JK, Gupta N, Alaraj S, Daoud A. Compressive characteristics of A356/fly ash cenosphere composites synthesized by pressure infiltration technique. *Compos Part A Appl Sci Manuf.* (2006) **37**:430–7. doi: 10.1016/j.compositesa.2005.05.047
41. Singla YK, Chhibber R, Bansal H, Kalra A. Wear behavior of aluminum Alloy 6061-based composites reinforced with SiC, Al_2O_3, and red mud: a comparative study. *Jom.* (2015) **67**:2160–9. doi: 10.1007/s11837-015-1365-0
42. Shanmugavel R, Sundaresan TK, Marimuthu U, Manickaraj P. Process optimization and wear behavior of red mud reinforced aluminum composites. *Adv Tribol.* (2016) **2016**:7. doi: 10.1155/2016/9082593
43. Rao RG, Ghosh M, Ganguly RI, Bose PSC, Sahoo KL. Mechanical properties and age hardening response of Al6061 alloy based composites reinforced with fly ash. *Mater Sci Eng A.* (2020) **772**:138823. doi: 10.1016/j.msea.2019.138823
44. Arunachalam S, Chelladurai SJS. Optimization of dry sliding wear parameters of AA336 aluminum alloy-boron carbide and fly ash reinforced hybrid composites by stir casting process. *Materwiss Werksttech.* (2020) **51**:189–98. doi: 10.1002/mawe.201900069
45. Manikandan R, Arjunan TV, Akhil AR. Studies on micro structural characteristics, mechanical and tribological behaviours of boron carbide and cow dung ash reinforced aluminum (Al 7075) hybrid metal matrix composite. *Compos Part B Eng.* (2020) **183**:107668. doi: 10.1016/j.compositesb.2019.107668
46. Sagar KG, Suresh PM, Nataraj JR. Effect of beryl reinforcement in aluminum 2024 on mechanical properties. *J Inst Eng Ser C.* (2020) **101**:507–16. doi: 10.1007/s40032-020-00554-x
47. Hashim J, Looney L, Hashmi MSJ. Metal matrix composites: production by the stir casting method. *J Mater Process Technol.* (1999) **92–93**:1–7. doi: 10.1016/S0924-0136(99)00118-1
48. Ravi KR, Sreekumar VM, Pillai RM, Mahato C, Amaranathan KR, Arul kumar R, et al. Optimization of mixing parameters through a water model for metal matrix composites synthesis. *Mater Des.* (2007) **28**:871–81. doi: 10.1016/j.matdes.2005.10.007
49. Kalaiselvan K, Murugan N, Parameswaran S. Production and characterization of AA6061-B4C stir cast composite. *Mater Des.* (2011) **32**:4004–9. doi: 10.1016/j.matdes.2011.03.018
50. Toptan F, Kilicarslan A, Karaaslan A, Cigdem M, Kerti I. Processing and microstructural characterisation of AA 1070 and AA 6063 matrix B4Cp reinforced composites. *Mater Des.* (2010) **31**:S87–91. doi: 10.1016/j.matdes.2009.11.064
51. Rohatgi PK, Kim JK, Guo RQ, Robertson DP, Gajdardziska-Josifovska M. Age-hardening characteristics of aluminum alloy-hollow fly ash composites. *Metall Mater Trans A Phys Metall Mater Sci.* (2002) **33**:1541–7. doi: 10.1007/s11661-002-0076-7
52. Zahi S, Daud AR. Fly ash characterization and application in Al-based Mg alloys. *Mater Des.* (2011) **32**:1337–46. doi: 10.1016/j.matdes.2010.09.021
53. Kalaiselvan K, Dinaharan I, Murugan N. Characterization of friction stir welded boron carbide particulate reinforced AA6061 aluminum alloy stir cast composite. *Mater Des.* (2014) **55**:176–82. doi: 10.1016/j.matdes.2013.09.067
54. Sahu MK. Fabrication of of aluminum aluminum matrix matrix composites composites by stir casting technique and stirring process parameters optimization. In: Vijayaram TR, editor. *Advanced Casting Techniques.* London: Intech Open (2018). p. 111–26.

55. Saravanan KK, Mahendran S. Aluminum 6082-boron carbide composite materials preparation and investigate mechanical-electrical properties with CNC turning. *Mater Today Proc.* (2020) **21**:93–7. doi: 10.1016/j.matpr.2019.05.368
56. Faisal MH, Prabagaran S. Investigation on mechanical and wear properties of aluminum based metal matrix composite reinforced with B4C, Gr and Fly Ash. In *Advanced Manufacturing and Materials Science.* Cham: Springer (2018). p. 379–85. doi: 10.1007/978-3-319-76276-0_38
57. Bhaskar Kurapati V, Kommineni R, Sundarrajan S. Statistical Analysis and mathematical modeling of dry sliding wear parameters of 2024 aluminum hybrid composites reinforced with fly ash and SiC particles. *Trans Indian Inst Met.* (2018) **71**:1809–25. doi: 10.1007/s12666-018-1322-z
58. Baradeswaran A, Vettivel SC, Elaya Perumal A, Selvakumar N, Franklin Issac R. Experimental investigation on mechanical behaviour, modelling and optimization of wear parameters of B4C and graphite reinforced aluminum hybrid composites. *Mater Des.* (2014) **63**:620–32. doi: 10.1016/j.matdes.2014.06.054
59. Satheesh Raja R, Manisekar K. Experimental and statistical analysis on mechanical properties of nano flyash impregnated GFRP composites using central composite design method. *Mater Des.* (2016) **89**:884–92. doi: 10.1016/j.matdes.2015.10.043
60. Gajalakshmi K, Senthilkumar N, Prabu B. Multi-response optimization of dry sliding wear parameters of AA6026 using hybrid gray relational analysis coupled with response surface method. *Meas Control.* (2019) **52**:540–53. doi: 10.1177/0020294019842603
61. Davim JP. *Design of Experiments in Production Engineering.* Cham: Springer (2016). doi: 10.1007/978-3-319-23838-8
62. Vettivel SC, Selvakumar N, Narayanasamy R, Leema N. Numerical modelling, prediction of Cu-W nano powder composite in dry sliding wear condition using response surface methodology. *Mater Des.* (2013) **50**:977–96. doi: 10.1016/j.matdes.2013.03.072
63. Ramkumar SSKR, Al FA, Osama M. Effect of - TiB 2 / Gr hybrid reinforcements in Al 7075 matrix on sliding wear behavior analyzed by response surface methodology. *Met Mater Int.* (2019). doi: 10.1007/s12540-019-00543-5. [Epub ahead of print].
64. Raj R. Effect of particle size and volume fraction on the strengthening mechanisms of boron carbide reinforced aluminum metal matrix composites. *J Mech Eng. Sci.* (2018) **233**:1345–56. doi: 10.1177/0954406218771997
65. Fan LJ, Juang SH. Reaction effect of fly ash with Al-3Mg melt on the microstructure and hardness of aluminum matrix composites. *Mater Des.* (2016) **89**:941–9. doi: 10.1016/j.matdes.2015.10.070
66. Reddy PS, Vijaya R, Kesavan R. Investigation of mechanical properties of aluminum 6061-Silicon carbide, boron carbide metal matrix composite. *Silicon.* (2018) 10:495–502. doi: 10.1007/s12633-016-9479-8
67. Zheng J, Li Q, Liu W, Shu G. Microstructure evolution of 15 wt% boron carbide/aluminum composites during liquid-stirring process. *J Compos Mater.* (2016) **50**:3843–52. doi: 10.1177/0021998315626258
68. Canute X, Majumder MC. Mechanical and tribological behaviour of stir cast aluminum / boron carbide / fly ash composites. *J Eng Sci Technol.* (2018) **13**:755–77.
69. Manoj MK, Gadpale V. Synthesis, characterization and dry sliding wear behaviour of Al 7075–MoSi2 composites prepared by stir casting technique. *Trans Indian Inst Met.* (2019) **72**:3153–69. doi: 10.1007/s12666-019-01781-2
70. Singh G, Goyal S. Dry sliding wear behaviour of AA6082-T6/SiC/B4C hybrid metal matrix composites using response surface methodology. *Proc Inst Mech Eng Part L J Mater Des Appl.* (2018) **232**:952–64. doi: 10.1177/1464420716657114
71. Davanageri MB, Narendranath S, Kadoli R. Modeling and optimization of wear rate of AISI 2507 super duplex stainless steel. *Silicon.* (2019) **11**:1023–34. doi: 10.1007/s12633-018-9908-y
72. Sharma P, Khanduja D, Sharma S. Dry sliding wear investigation of Al6082/Gr metal matrix composites by response surface methodology. *J Mater Res Technol.* (2016) **5**:29–36. doi: 10.1016/j.jmrt.2015.05.001
73. Chelladurai SJS, Arthanari R, Selvarajan R, Ravichandran TP, Ravi SK, Petchimuthu SRC. Optimisation of dry sliding wear parameters of squeeze cast AA336 aluminum alloy: copper-coated steel wire-reinforced composites by response surface methodology. *Int J Met.* (2019) **13**:354–66. doi: 10.1007/s40962-018-0258-8
74. Raghavendra CR, Basavarajappa S, Sogalad I. Optimization of wear parameters on Ni–Al2O3 nanocomposite coating by electrodeposition process. *SN Appl Sci.* (2019) **1**:1–8. doi: 10.1007/s42452-018-0135-3
75. Sinha AK, Bhattacharya S, Narang HK. Experimental determination and modelling of the mechanical properties of hybrid abaca-reinforced polymer composite using RSM. *Polym Polym Compos.* (2019) 27:096739111985584. doi: 10.1177/0967391119855843
76. Ahmadi M, Vahabzadeh F, Bonakdarpour B, Mofarrah E, Mehranian M. Application of the central composite design and response surface methodology to the advanced treatment of olive oil processing wastewater using Fenton's peroxidation. *J Hazard Mater.* (2005) **123**:187–95. doi: 10.1016/j.jhazmat.2005.03.042
77. Lakshminarayanan AK, Balasubramanian V. Comparison of RSM with ANN in predicting tensile strength of friction stir welded AA7039 aluminum alloy joints. *Trans Nonferrous Met Soc China.* (2009) **19**:9–18. doi: 10.1016/S1003-6326(08)60221-6
78. Balasubramanian M. Developing mathematical models to predict tensile properties of pulsed current gas tungsten arc welded Ti – 6Al – 4V alloy. *Mater Design.* (2008) **29**:92–7. doi: 10.1016/j.matdes.2006.12.001
79. Rajakumar S, Muralidharan C, Balasubramanian V. Establishing empirical relationships to predict grain size and tensile strength of friction stir welded AA 6061-T6 aluminum alloy joints. *Trans Nonferrous Met Soc China.* (2010) **20**:1863–72. doi: 10.1016/S1003-6326(09)60387-3
80. Velmanirajan K, Abu AS, Narayanasamy R, Basha CA. Numerical modelling of aluminum sheets formability using response surface methodology. *Mater Des.* (2012) **41**:239–54. doi: 10.1016/j.matdes.2012.05.027
81. Kumar CR, Malarvannan RRR, JaiGanesh V. Role of SiC on mechanical, tribological and thermal expansion characteristics of B4C/Talc-Reinforced Al-6061 hybrid composite. *Silicon.* (2020) **12**:1491–500. doi: 10.1007/s12633-019-00243-0
82. Sadagopan P, Natarajan HK, Praveen Kumar J. Study of silicon carbide-reinforced aluminum matrix composite brake rotor for motorcycle application. *Int J Adv Manuf Technol.* (2018) **94**:1461–75. doi: 10.1007/s00170-017-0969-7

Conflict of Interest: The authors declare that the research was conducted in the absence of any commercial or financial relationships that could be construed as a potential conflict of interest.